A Graphical Model Framework for Coupling MRFs and Deformable Models

Rui Huang, Vladimir Pavlovic, and Dimitris N. Metaxas
Division of Computer and Information Sciences, Rutgers University
{ruihuang, vladimir, dnm}@cs.rutgers.edu

Abstract

This paper proposes a new framework for image segmentation based on the integration of MRFs and deformable models using graphical models. We first construct a graphical model to represent the relationship of the observed image pixels, the true region labels and the underlying object contour. We then formulate the problem of image segmentation as the one of joint region-contour inference and learning in the graphical model. The graphical model representation allows us to use an approximate structured variational inference technique to solve this otherwise intractable joint inference problem. Using this technique, the MAP solution to the original model is obtained by finding the MAP solutions of two simpler models, an extended MRF model and a probabilistic deformable model, iteratively and incrementally. In the extended MRF model, the true region labels are estimated using the BP algorithm in a band area around the estimated contour from the probabilistic deformable model, and the result in turn guides the probabilistic deformable model to an improved estimation of the contour. Experimental results show that our new hybrid method outperforms both the MRF-based and the deformable model-based methods.

1. Introduction

Image segmentation is one of the most important and difficult preliminary processes for high-level computer vision and pattern recognition problems. The main goal of image segmentation is to divide an image into its constituent parts that have a strong correlation with objects or areas of the real world depicted by the image.

Region-based and edge-based segmentations are the two major classes of segmentation methods. Though one can label regions according to edges or detect edges from regions, these two kinds of methods are naturally different and have respective advantages and disadvantages.

Region-based methods assign image pixels to a region according to some image property (e.g., region homogeneity). These methods work well in noisy images, where edges are usually difficult to detect while the region homogeneity is preserved. The disadvantages of region-based methods are that they may generate rough edges and holes inside the objects, and they do not take account of object shape.

On the other hand, edge-based methods generate boundaries of the segmented objects. A prior knowledge of object shape and topology can be easily incorporated to constrain the segmentation result. While this often leads to sufficiently smooth boundaries, the oversmoothing may be excessive. Because edge-based methods rely on edge detecting operators, they are sensitive to image noise and need to be initialized close to the actual region boundaries.

A hybrid segmentation method that combines region-based and edge-based methods may improve the segmentation results over the two methods alone. In this paper we propose a hybrid segmentation framework to combine the Markov Random Field (MRF)-based and the deformable model-based segmentation methods. To tightly couple the two models, we construct a graphical model to represent the relationship of the observed image pixels, the true region labels and the underlying object contour. Exact inference in the graphical model is intractable because of the large state spaces and the couplings of model variables. To tackle this problem we use a variational inference method to *seemingly* decouple the graphical model into two simpler models: one extended MRF model and one probabilistic deformable model. Then we obtain the MAP solution in the original model by solving the MAP problems of the two simpler models iteratively and incrementally. In the extended MRF model, the true region labels are estimated using the Belief Propagation (BP) algorithm in a band area around the estimated contour from the probabilistic deformable model, and the result in turn guides the probabilistic deformable model to an improved estimation of the contour.

The rest of this paper is organized as follows: section 2 reviews the previous work; section 3 introduces a new integrated model and its decoupled approximation using the variational inference method; detailed inferences on the decoupled models are described in section 4; section 5 shows the experimental results; and section 6 summarizes the paper and future work.

Proceedings of the 2004 IEEE Computer Society Conference on Computer Vision and Pattern Recognition (CVPR'04)
1063-6919/04 $20.00 © 2004 **IEEE**

2. Previous work

Most segmentation methods are either region-based or edge-based. Among region-based methods, besides the classical region growing method [1], the MRF-based methods have been extensively used in different areas [2][3][4]. Because the exact MAP inference in MRF models is computationally infeasible, various techniques for approximating the MAP estimation have been proposed, such as Markov Chain Monte Carlo (MCMC) [5], iterated conditional modes (ICM) [6], maximizer of posterior marginals (MPM) [7], etc. Reference [8] presents a comparative analysis of some of these methods.

In edge-based methods, since Kass et al. introduced Snakes [9], deformable models have attracted much attention. Variants of deformable models have been proposed to address different problems. For instance, Balloons [10] and Gradient Vector Flow (GVF) Snakes [11] introduces different external forces, and topologically adaptable Snakes [12] allow changes in the model's topology. See [13] for a review of deformable models and [1] for other edge-based methods and some basic edge detecting operators.

Hybrid approaches [14][15][16] attempt to combine region-based and edge-based segmentations to alleviate deficiencies of the individual methods. There are different choices of the combination. For instance, [16] proposes a way of integrating MRFs and deformable models. MRFs are used to initially estimate the boundary of objects in noisy images. Balloons are then fitted to the estimated boundary. The result of the fitting is in turn used to update the MRF parameters. Final segmentation is achieved by iteratively integrating these processes.

While this hybrid method attempted to take advantage of both MRFs and deformable models, the model coupling was loose. This may cause failure of deformable models if the initial estimation of the boundary by MRF is not closed, and it may also yield oversmoothed boundaries.

3. Our method

We propose a new framework to combine MRFs and deformable models. The goal of our segmentation method is to find one specific region with a smooth and closed boundary. A seed point is manually specified and the region containing it is then segmented automatically. Thus, without significant loss of modeling generality, we simplify the MRF model and avoid possible problems caused by segmenting multiple regions simultaneously.

In this section, we first briefly review MRFs and deformable models, define the notation, and then introduce our hybrid framework.

3.1. MRF-based segmentation

MRF models are often used for image segmentation, because of their ability to capture the context of an image (i.e., dependencies among neighboring image pixels) and deal with the noise.

A typical MRF model for image segmentation, as shown in Figure 1, is a graph with two kinds of nodes: hidden nodes (circles in Figure 1, representing region labels) and observable nodes (squares in Figure 1, representing image pixels). Edges in the graph depict relationships among the nodes.

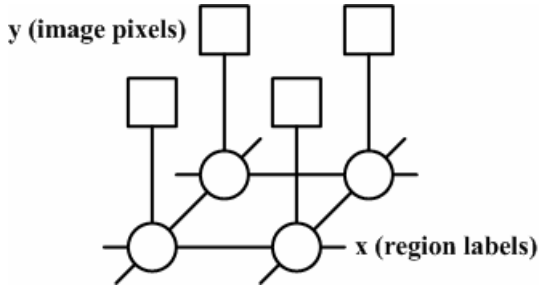

Figure 1. MRF model

Let n be the number of the hidden/observable states (i.e., the number of pixels in the image). A configuration of the hidden layer is:

$$\mathbf{x} = (x_1, ..., x_n), x_i \in L, i = 1, ..., n \quad (1)$$

where L is a set of region labels, such as L = {*inside*, *outside*}.

Similarly, a configuration of the observable layer is:

$$\mathbf{y} = (y_1, ..., y_n), y_i \in D, i = 1, ..., n \quad (2)$$

where D is a set of pixel values, e.g., gray values 0-255.

The relationship between the hidden states and the observable states (also known as local evidence) can be represented as the compatibility function:

$$\phi(x_i, y_i) = P(y_i \mid x_i) \quad (3)$$

Similarly, the relationship between the neighboring hidden states can be represented as the second compatibility function:

$$\psi(x_i, x_j) = P(x_i, x_j) \quad (4)$$

Now the segmentation problem can be viewed as a problem of estimating the MAP solution of the MRF model:

$$\mathbf{x}_{MAP} = \arg\max_{\mathbf{x}} P(\mathbf{x} \mid \mathbf{y}) \quad (5)$$

where

$$P(\mathbf{x} \mid \mathbf{y}) \propto P(\mathbf{y} \mid \mathbf{x}) P(\mathbf{x}) \propto \prod_i \phi(x_i, y_i) \prod_{(i,j)} \psi(x_i, x_j) \quad (6)$$

As mentioned previously, the exact MAP inference in MRF models is computationally infeasible, and various techniques have been used for approximating the MAP estimation. In our method, we use the BP algorithm. The

estimation of the MRF parameters (i.e., the parameters in the compatibility functions) is another related problem, often solved using the EM algorithm [3]. However, in the presence of multiple regions in the image, the automatic determination of the number of regions and the initial guess of the parameters could be difficult. More importantly, like other region-based methods, MRFs do not take account of object shape and may generate rough edges and even holes inside the objects.

3.2. Deformable model-based segmentation

Many deformable model-based methods have also been used in segmentation. A deformable model is usually a parameterized geometric primitive, whose deformation is determined by geometry, kinematics, dynamics and other constraints (e.g., material properties, etc.) [17]. Snakes [9], a special case of deformable models, are a parametric contour:

$$\Omega = [0,1] \to \Re^2,$$
$$s \to \mathbf{c}(s) = (x(s), y(s)),$$

where s is the parametric domain and x and y are the coordinate functions. The energy of the contour:

$$E(\mathbf{c}) = E_{\text{int}}(\mathbf{c}) + E_{\text{ext}}(\mathbf{c}) = \int_{\Omega} \omega_1(s)\left|\frac{\partial \mathbf{c}}{\partial s}\right|^2 + \omega_2(s)\left|\frac{\partial^2 \mathbf{c}}{\partial s^2}\right|^2 + F(\mathbf{c}(s))ds \quad (7)$$

where $\omega_1(s)$ and $\omega_2(s)$ control the "elasticity" and "rigidity" of the contour, and F is the potential associated to the external forces. The final shape of the contour corresponds to the minimum of this energy.

To minimize the above energy term, one can use the discretized first order Lagrangian dynamics equation:

$$\dot{\mathbf{d}} + \mathbf{K}\mathbf{d} = \mathbf{f} \quad (8)$$

where $\mathbf{d}$ is discretized version of $\mathbf{c}$, $\mathbf{K}$ is the stiffness matrix calculated from $\omega_1(s)$ and $\omega_2(s)$, and $\mathbf{f}$ is the generalized force vector.

Image gradient forces are usually used to attract a deformable model to edges. However, when far from the true boundary, the model often gets attracted to spurious image edges. Balloon forces have been introduced to solve this problem [10]. Namely, the deformable model is considered a balloon, which is inflated by an additional force and stopped by strong edges. The initial contour need no longer be close to the true boundary. Mathematically, a force along the normal direction to the curve at contour node $\mathbf{c}(s)$ with some appropriate amplitude k is added to the original forces.

$$\mathbf{f}' = \mathbf{f} + k\vec{\mathbf{n}}(s) \quad (9)$$

Deformable models can also be viewed in a probabilistic framework [13]. The internal energy $E_{\text{int}}(\mathbf{c})$ leads to a Gibbs prior distribution of the form:

$$P(\mathbf{c}) = \frac{1}{Z_i}\exp(-E_{\text{int}}(\mathbf{c})) \quad (10)$$

while the external energy $E_{\text{ext}}(\mathbf{c})$ can be converted to a sensor model with conditional probability:

$$P(\mathbf{I} \mid \mathbf{c}) = \frac{1}{Z_e}\exp(-E_{\text{ext}}(\mathbf{c})) \quad (11)$$

where $\mathbf{I}$ denotes the image, and $E_{\text{ext}}(\mathbf{c})$ is a function of the image $\mathbf{I}$.

The deformable models can now be fitted by solving the MAP problem:

$$\mathbf{c}_{MAP} = \arg\max_{\mathbf{c}} P(\mathbf{c} \mid \mathbf{I}) \quad (12)$$

where

$$P(\mathbf{c} \mid \mathbf{I}) \propto P(\mathbf{c})P(\mathbf{I} \mid \mathbf{c}) \quad (13)$$

One limitation of the deformable model-based method is its sensitivity to image noise, a common drawback of edge-based methods. This may result in the deformable model being "stuck" in a local energy minimum of a noisy image.

3.3. Integrated model

As shown in equation (5) and (12), both the MRF-based and the deformable model-based segmentations can be viewed as the MAP estimation problems. In previous work [16], these two models were loosely coupled. Our new framework uses the graphical model theory to tightly couple the two models. This is achieved, as depicted in Figure 2, by adding a new hidden state to the traditional MRF model to represent the underlying contour.

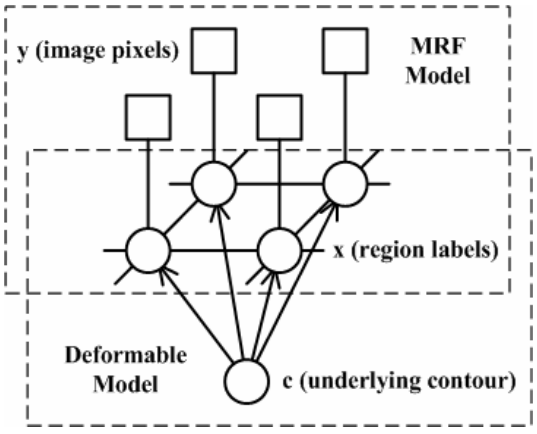

Figure 2. Integrated model

In the new model, the segmentation problem can also be viewed as a *joint* MAP estimation problem:

$$(\mathbf{c}, \mathbf{x})_{MAP} = \arg\max_{\mathbf{c},\mathbf{x}} P(\mathbf{c}, \mathbf{x} \mid \mathbf{y}) \quad (14)$$

where

$$P(\mathbf{c}, \mathbf{x} \mid \mathbf{y}) \propto P(\mathbf{y} \mid \mathbf{x})P(\mathbf{x} \mid \mathbf{c})P(\mathbf{c}) \quad (15)$$

To define the joint distribution of the integrated model, we model the image likelihood term $P(\mathbf{y}\,|\,\mathbf{x})$ as:

$$P(\mathbf{y}\,|\,\mathbf{x}) = \prod_i P(y_i\,|\,x_i) = \prod_i \phi(x_i, y_i) \tag{16}$$

identical to the traditional MRF model.

The second term $P(\mathbf{x}\,|\,\mathbf{c})$, modeling the distribution of the region labels conditioned on the contour, is defined as:

$$\begin{aligned} P(\mathbf{x}\,|\,\mathbf{c}) &= \prod_{(i,j)} P(x_i, x_j) \prod_i P(x_i\,|\,\mathbf{c}) \\ &= \prod_{(i,j)} \psi(x_i, x_j) \prod_i P(x_i\,|\,\mathbf{c}) \end{aligned} \tag{17}$$

where we incorporated a shape prior **c** to constrain the region labels **x**, in addition to the original Gibbs distribution. Since we only segment one specific region at one time, we need only consider the pixels near the contour, and label them either *inside* or *outside* the contour. Now we can model the dependency between the contour **c** and the region labels **x** using the softmax function:

$$P(x_i = inside\,|\,\mathbf{c}) = \frac{1}{1 + \exp(-dist(i, \mathbf{c}))} \tag{18}$$

$$P(x_i = outside\,|\,\mathbf{c}) = 1 - P(x_i = inside\,|\,\mathbf{c}) \tag{19}$$

induced by the signed Chamfer distance of pixel *i* from the contour **c**:

$$dist(i, \mathbf{c}) = sign(i, \mathbf{c}) \min_{s \in \Omega} \left\| loc(i) - \mathbf{c}(s) \right\| \tag{20}$$

where $sign(i, \mathbf{c}) = 1$ if pixel *i* is inside contour **c**; $sign(i, \mathbf{c}) = -1$ when it is outside, and $loc(i)$ denotes the spatial coordinates of pixel *i*.

Lastly, the prior term $P(\mathbf{c})$, as in equation (10), can be represented as a Gibbs distribution when the shape prior is given by a parametric contour **c**.

Despite the compact graphical representation of the integrated model, the exact inference in the model is computationally intractable. One reason for this is the large state space size and the complex dependency structure introduced by the Gibbs distribution of the prior $P(\mathbf{c})$. The second reason is the existence of loops in the graphical model, which preclude polynomial-time inference. To deal with these problems we propose an approximate, yet tractable, solution based on structured variational inference.

3.4. Approximate inference using structured variational inference

Structured variational inference techniques [18][19] consider parameterized distribution which is in some sense close to the desired posterior distribution, but is easier to compute. Namely, for a given image **y**, a distribution $Q(\mathbf{c}, \mathbf{x}\,|\,\mathbf{y}, \theta)$ with an additional set of *variational parameters* θ is defined such that the Kullback–Leibler divergence between $Q(\mathbf{c}, \mathbf{x}\,|\,\mathbf{y}, \theta)$ and $P(\mathbf{c}, \mathbf{x}\,|\,\mathbf{y})$ is minimized with respect to θ:

$$\theta^* = \arg\min_{\theta} \sum_{\mathbf{c},\mathbf{x}} Q(\mathbf{c}, \mathbf{x}\,|\,\mathbf{y}, \theta) \log \frac{P(\mathbf{c}, \mathbf{x}\,|\,\mathbf{y})}{Q(\mathbf{c}, \mathbf{x}\,|\,\mathbf{y}, \theta)} \tag{21}$$

The dependency structure of Q is chosen such that it closely resembles the dependency structure of the original distribution *P*. However, unlike *P* the dependency structure of Q *must* allow a computationally efficient inference.

In our case we define Q by decoupling the MRF model and the deformable model components of the original integrated model in Figure 2. The original distribution is factorized into two independent distributions: an extended MRF model Q_M with variational parameter **a** and a deformable model Q_D with variational parameter **b** (Figure 3). The *extended* MRF model means we have an additional layer to the traditional MRF model to deal with the shape prior.

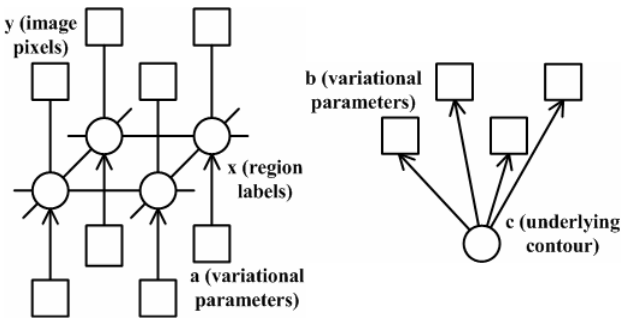

Figure 3. Decoupled models

Because Q_M and Q_D are independent,

$$Q(\mathbf{c}, \mathbf{x}\,|\,\mathbf{y}, \mathbf{a}, \mathbf{b}) = Q_M(\mathbf{x}\,|\,\mathbf{y}, \mathbf{a}) Q_D(\mathbf{c}\,|\,\mathbf{b}) \tag{22}$$

According to the extended MRF model, we have:

$$Q_M(\mathbf{x}\,|\,\mathbf{y}, \mathbf{a}) \propto Q_M(\mathbf{y}\,|\,\mathbf{x}) Q_M(\mathbf{x}\,|\,\mathbf{a}) \tag{23}$$

$$Q_M(\mathbf{y}\,|\,\mathbf{x}) = \prod_i P(y_i\,|\,x_i) = \prod_i \phi(x_i, y_i) \tag{24}$$

$$\begin{aligned} Q_M(\mathbf{x}\,|\,\mathbf{a}) &= \prod_{(i,j)} P(x_i, x_j) \prod_i P(x_i\,|\,a_i) \\ &= \prod_{(i,j)} \psi(x_i, x_j) \prod_i P(x_i\,|\,a_i) \end{aligned} \tag{25}$$

Hence,

$$Q_M(\mathbf{x}\,|\,\mathbf{y}, \mathbf{a}) \propto \prod_i \phi(x_i, y_i) \prod_{(i,j)} \psi(x_i, x_j) \prod_i P(x_i\,|\,a_i) \tag{26}$$

The deformable model yields:

$$Q_D(\mathbf{c}\,|\,\mathbf{b}) \propto Q_D(\mathbf{b}\,|\,\mathbf{c}) Q_D(\mathbf{c}) \tag{27}$$

$$Q_D(\mathbf{b}\,|\,\mathbf{c}) = \prod_i P(b_i\,|\,\mathbf{c}) \tag{28}$$

leading to

$$Q_D(\mathbf{c}\,|\,\mathbf{b}) \propto \prod_i P(b_i\,|\,\mathbf{c}) Q_D(\mathbf{c}) \tag{29}$$

The optimal values of the variational parameters $\theta = (\mathbf{a}, \mathbf{b})$ are obtained by minimizing the KL-divergence. It can be shown, using e.g., [20], that the optimal parameters $\theta^* = (\mathbf{a}^*, \mathbf{b}^*)$ should satisfy the following equations:

$$\log P(x_i \mid a_i^*) = \sum_{\mathbf{c}} Q_D(\mathbf{c} \mid \mathbf{b}^*) \log P(x_i \mid \mathbf{c}) \quad (30)$$

$$\log P(b_i^* \mid \mathbf{c}) = \sum_{x_i \in L} Q_M(x_i \mid \mathbf{y}, \mathbf{a}^*) \log P(x_i \mid \mathbf{c}) \quad (31)$$

To obtain the term $Q_M(x_i \mid \mathbf{y}, \mathbf{a})$ we use the inference in the extended MRF with *soft* inputs **a** contributing according to $P(x_i \mid a_i)$. On the other hand, to compute $Q_D(\mathbf{c} \mid \mathbf{b})$ one would have to find the distribution of all contours **c** given the "label image" energy landscape $-\log P(\mathbf{b} \mid \mathbf{c})$, according to equation (11).

Since the state space of **c** is too large, we simply use winner-take-all strategy and approximate $Q_D(\mathbf{c} \mid \mathbf{b})$ as a delta function:

$$Q_D{}'(\mathbf{c} \mid \mathbf{b}) = \begin{cases} 1 \text{ if } \mathbf{c} = \arg\max_{\mathbf{c}} Q_D(\mathbf{c} \mid \mathbf{b}) \\ 0 \text{ else} \end{cases} \quad (32)$$

and equation (30) can be simplified to:

$$P(x_i \mid a_i^*) = P(x_i \mid \mathbf{c}) \quad (33)$$

Equations (31) and (33) together with the inference solutions form a set of *fixed-point equations*. Solution of this fixed-point set yields a tractable approximation to the intractable original posterior.

3.5. Algorithm description

Initialize contour **c**;
while (error > maxError) {

1. Calculate a band area **B** around **c**. Perform remaining steps inside **B**;
2. Calculate $P(x_i \mid a_i)$ based on equation (33) using **c**;
3. Estimate the MRF-MAP solution $Q_M(x_i \mid \mathbf{y}, \mathbf{a})$ based on equation (26) using $P(x_i \mid a_i)$;
4. Calculate $\log P(b_i \mid \mathbf{c})$ based on equation (31) using $Q_M(x_i \mid \mathbf{y}, \mathbf{a})$;
5. Fit a deformable model with balloon forces based on equation (29) using $\log P(b_i \mid \mathbf{c})$;

}

The variational inference algorithm for the hybrid MRF-DM model is summarized as above. Steps 2 and 4 follow directly from equations (33) and (31). The details of steps 1, 3 and 5 are discussed in next section.

4. Implementation issues

4.1. Solve MRF-MAP with EM and BP

Step 3 of our algorithm solves the MAP problem in the extended MRF Model. The EM algorithm is used to estimate both the MAP solution of region labels **x** and the parameters of the model.

Particularly, in E-step, the MAP solution of region labels **x** is estimated based on current parameters. Unlike most of the previous work mentioned in section 2, we solve this MRF-MAP estimation problem using the BP algorithm. BP is an inference method proposed by Pearl [21] to efficiently estimate Bayesian beliefs in the network by the way of iteratively passing messages between neighbors. It is an exact inference method in the network without loops. Even in the network with loops, the method often leads to good approximate and tractable solutions [22]. There are two variants of the BP algorithm: sum-product and max-product. The sum-product message passing rule can be written as:

$$m_{ij}(x_j) = \sum_{x_i} \Psi_{ij}(x_i, x_j) \Phi_i(x_i) \prod_{k \in \aleph(i) \setminus j} m_{ki}(x_i) \quad (34)$$

The max-product has analogous formula, with the marginalization replaced by the maximum operator. At convergence:

$$x_{iMAP} = \arg\max_{x_i} \Phi_i(x_i) \prod_{j \in \aleph(i)} m_{ji}(x_i) \quad (35)$$

According our extended MRF model the compatibility functions are:

$$\Phi_i(x_i) = P(y_i \mid x_i) P(x_i \mid a_i) = \phi(x_i, y_i) P(x_i \mid a_i) \quad (36)$$

$$\Psi_{ij}(x_i, x_j) = P(x_i, x_j) = \psi(x_i, x_j) \quad (37)$$

We again note the difference from a traditional MRF model, due to the incorporated shape prior. $P(x_i \mid a_i)$ is calculated in step 2 of the algorithm. $\phi(x_i, y_i)$ and $\psi(x_i, x_j)$ can be calculated using current MRF parameters.

In this model we assume the image pixels are corrupted by white Gaussian noise:

$$\phi(x_i, y_i) = \frac{1}{\sqrt{2\pi\sigma_{x_i}^2}} \exp\left(-\frac{(y_i - \mu_{x_i})^2}{2\sigma_{x_i}^2} \right) \quad (38)$$

On the other hand,

$$\psi(x_i, x_j) = \frac{1}{Z} \exp\left(\frac{\delta(x_i - x_j)}{\sigma^2} \right) \quad (39)$$

where $\delta(x) = 1$ if $x = 0$; $\delta(x) = 0$ if $x \neq 0$, σ controls the similarity of neighboring hidden states, and Z is a normalization constant.

As shown in step 1, in our algorithm belief propagation is restricted to a single band of model variables around the current contour estimates. A reason for this is that, in practice, we only need to care about the statistics of pixels near the boundary. More importantly, the banded inference significantly speeds up the whole algorithm. Although convergence of the banded algorithm is not

guaranteed, in our experiments, the BP algorithm does converge, usually in only one or two iterations.

In M-step, the MRF parameters are updated based on the MAP solution of region labels **x** using following equations:

$$\mu_l = \frac{\sum_i Q_M(x_i = l \mid y_i, a_i) y_i}{\sum_i Q_M(x_i = l \mid y_i, a_i)} \tag{40}$$

$$\sigma_l^2 = \frac{\sum_i Q_M(x_i = l \mid y_i, a_i)(y_i - \mu_l)^2}{\sum_i Q_M(x_i = l \mid y_i, a_i)} \tag{41}$$

where $l \in \{inside, outside\}$.

4.2. Probabilistic deformable model

In step 5, as mentioned in section 3.4, we use the negative log term, $-\log P(\mathbf{b} \mid \mathbf{c})$, as the external energy in the deformable model. In that case, the image force is simply $\nabla(\log P(\mathbf{b} \mid \mathbf{c}))$. With the additional balloon forces, this leads to the discretized first order Lagrangian dynamics equation:

$$\dot{\mathbf{d}} + \mathbf{K}\mathbf{d} = \nabla(\log P(\mathbf{b} \mid \mathbf{c})) + k\vec{\mathbf{n}}(s) \tag{42}$$

We note that this formulation is different from that of [16] where the deformable model is fitted to a binary image obtained from the MAP configuration of **x**. That is, the label of each pixel is fixed, i.e.,

$$P(\mathbf{b} \mid \mathbf{c}) = \max_{\mathbf{x}} P(\mathbf{x} \mid \mathbf{c}) \tag{43}$$

while in our method, we use a probabilistic measurement of label of each pixel as specified in equation (31).

Finally, following the definition in equations (18)~(20), we note that the gradient of the coupling energy at pixel *i*, $\nabla(\log P(\mathbf{b} \mid \mathbf{c}))$, can be shown to be:

$$\frac{\partial \log P(\mathbf{b} \mid \mathbf{c})}{\partial \mathbf{c}} = -\frac{\partial \log P(\mathbf{b} \mid \mathbf{c})}{\partial loc(i)} \tag{44}$$

5. Experiments

Our algorithm was implemented in MATLAB and all the experiments were tested on a 1.5GHz P4 Computer. Most of the experiments took less than one minute on the images of size 128×128 .

5.1. Synthetic images

The initial study of properties and utility of our method was conducted on a set of synthetic images. The images were synthesized in a way similar to [8]. In [8], the 64×64 perfect images contain only 2 gray levels representing the "object" (gray level is 160) and the "background" (gray level is 100) respectively. In our experiments, we made the background more complicated by introducing a gray level gradient. The gray levels of the background are increasing from 100 to 160, along the normal direction of the object contour (Figure 4a).

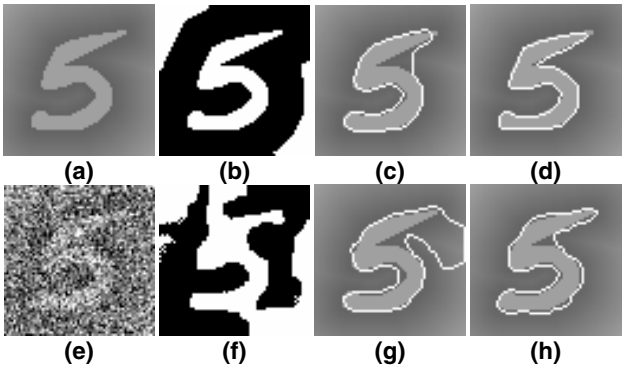

Figure 4. Experiments on synthetic images

Figure 4b shows the result of a traditional MRF-based method. The object is segmented correctly, however some regions in the background are misclassified. On the other hand, the deformable model fails because of the leaking from the high-curvature part of the object contour, where the gradient in the normal direction is too weak (Figure 4c). Our hybrid method, shown in Figure 4d, results in a significantly improved segmentation.

We next generated a test image (Figure 4e) by adding Gaussian noise with mean 0 and standard deviation 60 to Figure 4a. The result of the MRF-based method on the noisy image (Figure 4f) is somewhat similar to that in Figure 4b, which shows the MRF can deal with image noise to some extent. But significant misclassification occurred because of the complicated background and noise levels.

The deformable model either sticks to spurious edges caused by image noise or leaks (Figure 4g) because of the weakness of the true edges. Unlike the two independent methods, our hybrid algorithm, depicted in Figure 4h, correctly identifies the object boundaries despite the excessive image noise. For visualization purposes we superimpose the contour on the original image (Figure 4a) to show the quality of the result in Figures 4g and 4h.

5.2. Real images

Experiments with synthetic images in the previous section outlined some of the benefits of our hybrid method. The real world images usually have significant, often non-white noise and contain multiple regions and objects, rendering the segmentation task a great deal more difficult. In this section we show results of applying our method to real medical images on which we can hardly get satisfying results with either the MRF-based or the deformable model-based methods alone.

In the following comparisons, we manually specified the *inside*/*outside* regions to get an initial guess of the parameters for the MRF-only method. For the deformable model method, we started the balloon model at several different initial positions and use the best results for the comparison. On the other hand, our hybrid method is significantly less sensitive to the initialization of the parameters and the initial seed position.

Figure 5a shows a 2D MR image of the left ventricle of the human heart. Figure 5b is the result of the MRF-based method. While it is promising, the result still exhibits rough edges and holes. Figure 5c depicts the result of the deformable model-based method. Although we carefully chose the magnitude of the balloon forces, parts of the contour begin to leak others stick to spurious edges. Our hybrid method, started from the initial contour shown in Figure 5e, generated better result (Figure 5d). One of the intermediate iterations is shown in Figure 5f. The corresponding external energy in the band area is depicted in Figure 5g (gray values are proportional to the magnitude of the energy), showing a more useful profile than the traditional edge energy $-|\nabla(G_\sigma * I)|^2$ shown in Figure 5h.

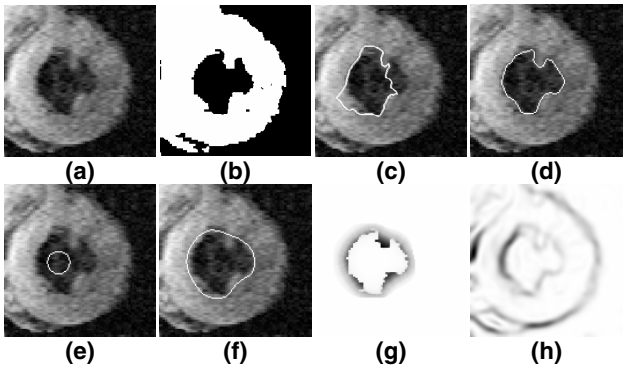

Figure 5. Experiments on medical images (1)

Figure 6a is an ultrasound image. The MRF gets rough edges and holes in the objects (Figure 6b) while the deformable model cannot escape a local minimum (Figure 6c). Our hybrid method eliminates the rough edges and holes caused by the MRF while outlining the region more accurately than the deformable model.

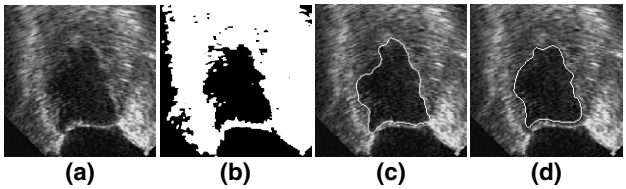

Figure 6. Experiments on medical images (2)

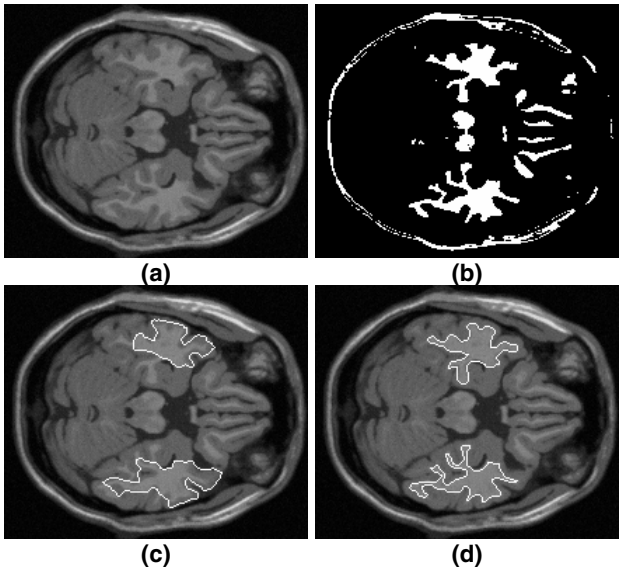

Figure 7. Experiments on medical images (3)

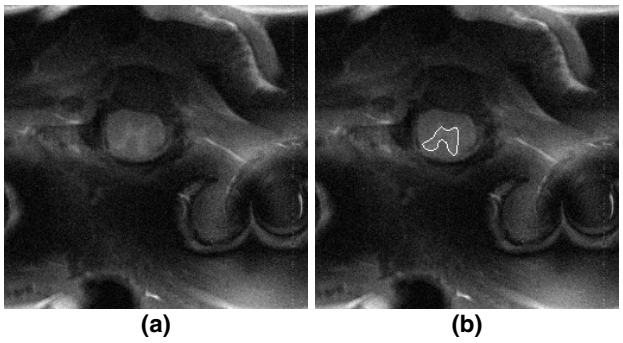

Figure 8. Experiments on medical images (4)

Finally, Figures 7a and 8a are both examples of difficult images with complicated global properties, requiring the MRF-based method to automatically determine the number of regions and the initial values of the parameters. Figure 7b is obtained by manually initializing the MRF model. Our method avoids this problem by creating and updating an MRF model locally and incrementally. The images are also difficult for deformable models because the boundaries of the objects to be segmented are either high-curvature (Figure 7a) or low-gradient (Figure 8a). Figure 7c exemplifies the over-smoothed deformable models. Our method's results, shown in Figures 7d and 8b, do not suffer from either of the problems.

6. Conclusions and future work

We proposed a new framework to combine the MRF-based and the deformable model-based segmentation methods. The framework was developed under the

auspices of the graphical model theory allowing us to employ a well-founded set of statistical estimation and learning techniques. In particular, we employed an approximate, computationally efficient solution to otherwise intractable inference of region boundaries. We showed the advantages and utility of our hybrid method on a number of synthetic and real-world images.

Our current method lacks adaptive parameter selection for both the deformable and the coupling model, an issue we plan to address in the future. Similarly, homogeneity of the MRF is a limiting factor that can be addressed using spatially-dependent models. Another interesting issue is how to apply other approximate inference algorithms, in particular belief propagation, to the whole model instead of the extended MRF alone. This may require a different representation of the probabilistic contour, possibly similar to [23] or [24]. Finally, the proposed framework can be extended to 3D segmentation as well as tracking problems requiring a shape prior, easily representable in our formalism.

Reference

[1] M. Sonka, V. Hlavac, and R. Boyle, *Image Processing, Analysis and Machine Vision, Second Edition*, PWS Publishing, 1998.

[2] K. Held, E.R. Kops, B.J. Krause, W.M. Wells III, R. Kikinis, and H.-W. Müller-Gärtner, "Markov Random Field Segmentation of Brain MR Images", *IEEE Transaction on Medical Imaging*, 16(6), 1997.

[3] Y. Zhang, M. Brady, and S. Smith, "Segmentation of Brain MR Images Through a Hidden Markov Random Field Model and the Expectation-Maximization Algorithm", *IEEE Transaction on Medical Imaging*, 20(1), 2001.

[4] A.K. Jain and S.G. Nadabar, "MRF Model-Based Segmentation of Range Images", *Proceedings of ICCV*, 1990.

[5] S. Geman and D. Geman, "Stochastic Relaxation, Gibbs Distributions and the Bayesian Restoration of Images", *IEEE Transaction on Pattern Analysis and Machine Intelligence*, 6(6), 1984.

[6] J. E. Besag, "On the Statistical Analysis of Dirty Pictures", *Journal of the Royal Statistical Society B*, 48(3), 1986.

[7] J. Marroquin, S. Mitter, and T. Poggio, "Probabilistic Solution of Ill-posed Problems in Computational Vision", *Journal of American Statistical Association*, 82(397), 1987.

[8] R.C. Dubes, A.K. Jain, S.G. Nadabar, and C.C. Chen, "MRF Model-Based Algorithm for Image Segmentation", *Proceedings of ICPR*, 1990.

[9] M. Kass, A. Witkin, and D. Terzopoulos, "Snakes: Active contour models", *International Journal of Computer Vision*, 1(4), 1987.

[10] L.D. Cohen, "On Active Contour Models and Balloons", *Computer Vision, Graphics, and Image Processing: Image Understanding*, 53(2), 1991.

[11] C. Xu and J.L. Prince, "Gradient Vector Flow: A New External Force for Snakes", *Proceedings of CVPR*, 1997.

[12] T. McInerney and D. Terzopoulos, "Topologically Adaptable Snakes", *Proceedings of ICCV*, 1995.

[13] T. McInerney and Demetri Terzopoulos, "Deformable Models in Medical Image Analysis: A Survey", *Medical Image Analysis*, 1(2), 1996.

[14] R. Ronfard, "Region-based Strategies for Active Contour Models", *International Journal of Computer Vision*, 13(2), 1994.

[15] T.N. Jones and D.N. Metaxas, "Image Segmentation Based on the Integration of Pixel Affinity and Deformable Models", *Proceedings of CVPR*, 1998.

[16] T. Chen and D.N. Metaxas, "Image Segmentation Based on the Integration of Markov Random Fields and Deformable Models", *Proceedings of MICCAI*, 2000.

[17] D.N. Metaxas, *Physics-based Deformable Models: Applications to Computer Vision, Graphics and Medical Imaging*, Kluwer Academic Press, 1997.

[18] M.I. Jordan, Z. Ghahramani, T. Jaakkola, and L.K. Saul, "An Introduction to Variational Methods for Graphical Models", *Machine Learning*, 37(2), 1999.

[19] V. Pavlovic, B.J. Frey, and T.S. Huang, "Variational Learning in Mixed-State Dynamic Graphical Models", *Proceedings of UAI*, 1999.

[20] Z. Ghahramani, "On Structured Variational Approximations", *Technical Report CRG-TR-97-1*, 1997.

[21] J. Pearl, *Probabilistic Reasoning in Intelligent Systems: Networks of Plausible Inference*, Morgan Kaufmann Publishers, 1988.

[22] Y. Weiss, "Belief Propagation and Revision in Networks with Loops", *Technical Report MIT A.I. Memo 1616*, 1998.

[23] Y. Chen, Y. Rui, and T. S. Huang, "JPDAF Based HMM for Real-Time Contour Tracking", *Proceedings of CVPR*, 2001.

[24] P. Pérez, A. Blake, and M. Gangnet, "JetStream: Probabilistic Contour Extraction with Particles", *Proceedings of ICCV*, 2001.